Available online at www.sciencedirect.com
SCIENCE DIRECT®
PERGAMON
Acta Astronautica 56 (2005) 439–452
ACTA ASTRONAUTICA
www.elsevier.com/locate/actaastro

Attitude control system for ROCSAT-3 microsatellite: a conceptual design

Y.W. Jan[a,b,*,1], J.C. Chiou[b,*]

[a] National Space Program Office, Hsinchu, Taiwan, ROC
[b] Department of Electrical and Control Engineering, National Chiao-Tung University, Hsinchu 30010, Taiwan, ROC

Received 15 April 2002; received in revised form 15 April 2004; accepted 4 May 2004

Abstract

The ROCSAT-3 attitude control subsystem is conceptually designed to meet the weight and power constraints of a microsatellite. Attractive features of the proposed design include (a) a control scheme for initial attitude acquisition, which provides a fully autonomous attitude hold, no duration limit and adequate attitude for power generation and (b) a feasible implementation for a microsatellite which has uncommon mission demands such as an orbit raising maneuver and practical weight and power constraints. The proposed control schemes for the three control modes and the spacecraft attitude dynamics are analyzed to demonstrate the satisfaction of the designated mission goals.

1. Introduction

The ROCSAT-3 consists of six micro-satellites with about 50 kg for each satellite. The six micro-satellites will form a constellation to provide a worldwide coverage. Fig. 1 gives a schematic representation of the constellation of twenty-four GPS satellites and the six ROCSAT-3 micro-satellites. The GPS Occultation Receiver is the primary payload for the ROCSAT-3's weather and climate research mission, which measures the temperature, pressure and some water content of the atmosphere utilizing the GPS satellites as a radio source [1]. The satellites will be launched by a single launcher into a low earth orbit to an altitude of approximately 475 km, and with an inclination angle of 72°. Orbit raising maneuvers will be performed to place satellites into the prescribed three orbit planes with altitude of 700 km. The longitudinal ascending nodes of the three orbital planes will be separated by approximately 60°.

The ROCSAT-3 attitude determination and control system (ADCS) will provide stable control and attitude knowledge throughout all phases of flight, from post-launch separation to deorbit maneuvers at the end of life. Specifically, the ADCS must

- provide three-axis attitude knowledge during both normal operations and during orbit-raising,
- hold a nadir-pointing orientation during normal operations (zero pitch, roll, and yaw angles),
- raise the satellite from a parking orbit to the final operational orbit using the thrusters,

* Corresponding author. Department of Electrical and Control Engineering, National Chiao-Tung University, Hsinchu 30010, Taiwan, ROC. Fax: +886-35-715-998.
E-mail addresses: ywjan@nspo.org.tw (Y.W. Jan), chiou@cc.nctu.edu.tw (J.C. Chiou).
[1] Researcher, Mechanical Engineering Department.

0094-5765/$ - see front matter © 2004 Elsevier Ltd. All rights reserved.
doi:10.1016/j.actaastro.2004.05.066

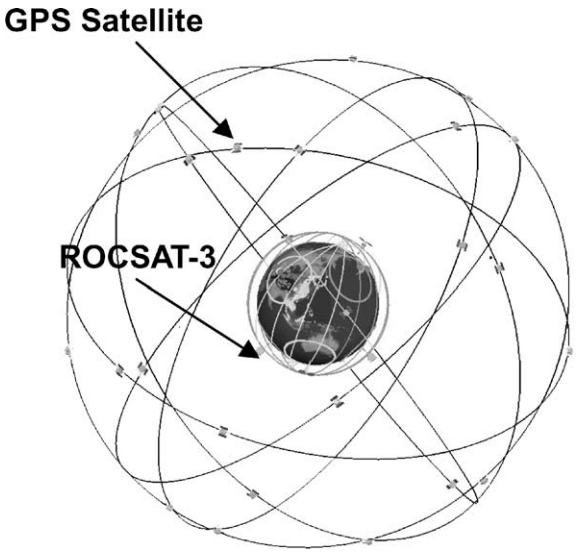

Fig. 1. ROCSAT-3 satellite and mission constellation schematic representation.

Table 1
Attitude determination and control requirements

Axis	Attitude determination (deg)	Attitude control (deg)
Pitch	±1	±2
Yaw	±2	±5
Roll	±2	±5

- transition the satellite from the post-launch separation conditions to a stable, nadir-pointing orientation,
- autonomously recover the satellite from a tumble to a safe orientation,
- build telemetry packages containing attitude knowledge and state-of-health,
- response to external commands (e.g., send telemetry data, change wheel speed setpoint, accept upload position vector, etc.),
- attitude determination and control requirements for normal operations are defined in Table 1.

2. ROCSAT-3 ADCS structure

The ADCS is designed to be "pitch momentum biased" with the boom structure nadir pointing. The subsystem contains an earth sensor, magnetometer and coarse sun sensors for determination, and a momentum wheel and three magnetic torque rods for control. The subsystem also has a coarse gyro for the short propulsion burns. Table 2 summarizes the ADCS hardware weight and power. The total weight is 3.15 kg and the average power for normal operations is 4 W.

Table 2
ADCS hardware summary

Assembly	Number per spacecraft	Unit weight (kg)	Total power (W)
Three-axis magnetometer	1	0.1	0.15
Solid state horizon sensor	2	0.4	0.5
Three-axis rate gyro	1	0.2	0.7
Two-axis coarse sun sensor	1	0.2	0.2
Magnetic torque rods	3	0.75	0.45
Pitch momentum wheel	1	1.5	2
Thrusters (really a major, subsystem but treated as actuators by ADCS)	4 4		

The control laws will be composed of three distinct modes: acquisition and SafeHold, normal operations, and orbit control.

(1) *SafeHold mode*: This is the mode to perform initial attitude acquisition, after launcher separation, and attitude recovery, following a failure detected. The SafeHold mode aims to ensure spacecraft safety without any ground support. The SafeHold mode performs rate reduction and sun acquisition using only simple equipment: magnetometer, coarse sun sensor, torque rods and momentum wheel. Neither thrusters nor gyroscopes are used. It is based on the use of a very simple magnetic control law, known as the "B-dot law", which induces energy dissipation. In the stationary state, the spacecraft sticks to the earth magnetic field, and hence rotates at twice the orbital rate. By creating an angular momentum with the wheel on pitch axis, the spacecraft rotates with respect to pitch axis so that the solar array faces the sun twice per orbit. It is then quite straightforward to perform sun acquisition, using only one coarse sun sensor. Therefore, the dynamics of the vehicle in the stationary state are (a) the spacecraft remains sun-pointed on the illuminated part of the orbit, and (b) during eclipse, magnetic control causes the spacecraft to perform one full revolution.

The use of such a concept has several advantages:

- It is fully autonomous, since navigation is not required.
- There is no hydrazine consumption. Hence, the duration of this mode is not limited. More, the orbit remains very stable.
- It is very robust, since the concept is very simple, requires no precision, and used only reliable equipment.

(2) *Normal operation mode*: The satellite will be nadir-pointing, with the roll, pitch and yaw angles near zero. The momentum wheel will be spinning in a direction to the orbit normal. The satellite will be in this mode while collecting GPS occultation data. The horizon sensor will provide pitch attitude information, and the magnetometer will provide attitude information perpendicular to the local magnetic field vector. The momentum wheel will be used to control the satellite pitch angle and to maintain the wheel speed at −0.2 N m s. The torque rods on roll and yaw axes will be used to dump wheel angular momentum. Roll and yaw control are achieved by commanding the pitch axis torque rod based on the magnetometer and horizon roll angle data.

(3) *Orbit control mode*: An initial three-axis attitude state will be established by using measurements from the magnetometer and horizon sensor. Gyro data will be used to propagate the attitude solution during the burn. The four thrusters nominally will all be firing to accomplish the orbit-raising objective. The thrusters will be selectively off-pulsed to provide three-axis attitude control during the burn, in addition to raising the orbit. The detailed thruster orientations are described in Section 4.3.

The ROCSAT-3's hydrazine propulsion system is a monopropellant blow-down type, with a bladder in the tank between the pressurant and the hydrazine. The tank carried 8 kg of fuel, which provided about 20% of margin. There are four fixed 1 N thrusters mounted on the side face of the satellite, canted 5° from the x-axis for roll control.

3. Attitude dynamics

Euler's equations in body coordinates for a spacecraft with internal angular momentum, h_x, h_y, h_z along the body X, Y, and Z-axes are [2]

$$\frac{\mathrm{d}}{\mathrm{d}t}\vec{L}+\vec{\omega}\times\vec{L}=\vec{N}_{\mathrm{E}}+\vec{N}_{\mathrm{C}}, \tag{1}$$

where $\vec{N}_{\mathrm{E}}$ and $\vec{N}_{\mathrm{C}}$ are the environmental and external control torques and the total angular momentum is $\vec{L}=\bar{I}\,\vec{\omega}+\vec{h}$.

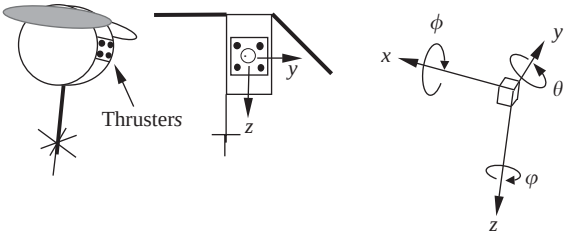

Fig. 2. The feature of ROCSAT-3 and definition of coordinates.

For a pitch momentum bias system, we have

$$\vec{h}=\begin{bmatrix}0\\-h_y\\0\end{bmatrix}$$

and we note that

$$h_y(t)=h_{\mathrm{B}}+\Delta h_{\mathrm{C}}(t),$$

where h_{B} is the pitch momentum bias and $\Delta h_{\mathrm{C}}(t)$ is the small variations in wheel momentum for pitch control.

For an earth pointing attitude with circular orbit, the body X-axis is along the velocity vector. The attitude angles are defined as roll, pitch and yaw, which are small rotational errors about the velocity vector, negative orbit normal, and nadir. The roll, pitch, and yaw angles are denoted by ϕ, θ, and ψ, respectively, as shown in Fig. 2. The transformation matrix from the orbit reference frame to the body frame is,

$$\bar{A}=\begin{bmatrix}1 & \psi & -\theta\\ -\psi & 1 & \phi\\ \theta & -\phi & 1\end{bmatrix}. \tag{2}$$

The angular velocity vector in the body frame is approximately

$$\vec{\omega}_{\mathrm{B}}=\begin{bmatrix}\dot{\phi}\\ \dot{\theta}\\ \dot{\psi}\end{bmatrix}+\bar{A}\begin{bmatrix}0\\-\omega_{\mathrm{o}}\\0\end{bmatrix}=\begin{bmatrix}\dot{\phi}-\omega_{\mathrm{o}}\psi\\ \dot{\theta}-\omega_{\mathrm{o}}\\ \dot{\psi}+\omega_{\mathrm{o}}\phi\end{bmatrix}, \tag{3}$$

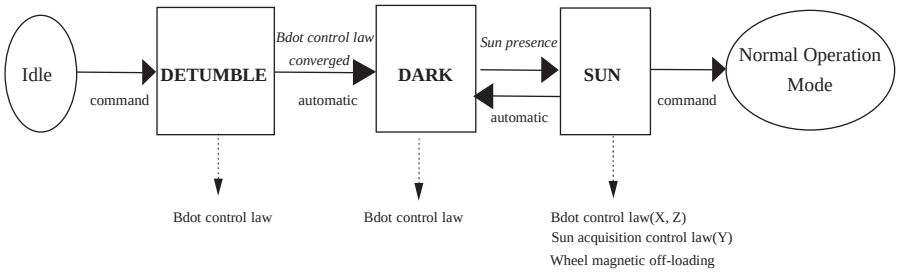

Fig. 3. SafeHold mode control law.

where ω_o is the orbital angular velocity of a spacecraft in a circular orbit.

Writing Eq. (1) in component form gives

$$I_x\ddot{\phi} + [\omega_o^2(I_y - I_z) - h_B\omega_o]\phi - [h_B - (I_x - I_y + I_z)\omega_o]\dot{\psi} = N_{Ex} + N_{Cx}, \tag{4a}$$

$$I_y\ddot{\theta} = N_{Ey} + N_{Cy}, \tag{4b}$$

$$I_z\ddot{\psi} + [\omega_o^2(I_x - I_y) - h_B\omega_o]\psi + [h_B - (I_x - I_y + I_z)\omega_o]\dot{\phi} = N_{Ez} + N_{Cx}. \tag{4c}$$

4. Control law design

4.1. SafeHold mode

The SafeHold mode is organized in 3 submodes and the control law corresponding to them is shown in Fig. 3.

- *Detumble submode*: stabilisation phase during which the initial rates are reduced by magnetic damping (Bdot control law),
- *Dark submode*: sun tracking phase during which the spacecraft follows the earth magnetic field, waiting for the sun. This phase is still controlled by magnetic damping (Bdot control law),
- *Sun submode*: sun locking phase during which the spacecraft is sun-pointed, controlled by both magnetic damping for X and Z-axes and wheel control for Y-axis (Bdot control law and sun acquisition control law).

4.1.1. Bdot control law (Detumble and Dark submodes)

As soon as the SafeHold mode is entered, the initial rates are reduced (in Detumble submode) using magnetometers, magneto-torquers and reaction wheel. The magnetic law, called Bdot control law is

$$\vec{M}_{mtq} = \frac{-K\dot{\vec{b}}}{\|\vec{B}\|} \tag{5}$$

with

$\vec{M}_{mtq}$= magnetic command,

$K = [Kx\ Ky\ Kz]$= Bdot law magnetic control gains,

$\vec{B}$= Earth magnetic field(measured by onboard magnetometer),

$\dot{\vec{b}}$= Earth magnetic field direction variation in ROCSAT-3. The control torque due to the magnetic command is given by

$$\vec{N}_c = \vec{M}_{mtq} \times \vec{B}. \tag{6}$$

This magnetic control law leads to a dynamic configuration where the spacecraft rotates at twice the orbital rate around the normal to orbit in order to follow the earth magnetic field evolution. In addition, an angular momentum bias is set by the wheel on the $-Y$ axis in order to set the rotation axis so that the solar array faces the sun twice per orbit. Therefore, once the Bdot law is converged, the spacecraft rotates at twice the orbital rate to stick the earth magnetic field. The $-Y$ axis of spacecraft is aligned with the normal to orbit plane.

In converged phase, MTQ X and Z control the pitch axis, whereas MTQ Y controls roll and yaw axes. The transition from Detumble to Dark submode is performed automatically when Bdot law is converged. The convergence criteria is based on the derivative of the earth magnetic field direction in ROCSAT-3. Indeed, this criteria is representative of the stationary state as the derivative is very low when the spacecraft sticks on the earth magnetic field.

4.1.2. Sun acquisition control law (Sun submode)

The sun acquisition stops the spacecraft rotation around the normal to orbit (i.e. Y_{sat}) so that the solar array faces the sun on the illuminated part of the orbit. The acquisition is performed using a coarse sun sensor and reaction wheel. The Sun submode is performed once in Dark submode (i.e. Bdot law converged) and when the sun is in the sun sensor field of view. During eclipse, Dark submode is recovered, which causes the spacecraft rotating at twice the orbital rate. During sun acquisition, Y-axis is controlled by reaction wheel. MTQ Y still controls X and Z-axes. MTQ X and Z (acting on Y-axis) are inhibited. During eclipse (in Dark submode), X, Y and Z-axes are all magnetic controlled.

The sun acquisition control law (around Y-axis) is

$$C_{Y\text{wheel}} = -K_e\alpha_y - K_v\dot{\alpha}_y \tag{7}$$

with

K_e, K_v = proportional and derivative control gains, α_y = pitch pointing error between $-Z_{sat}$ and the sun direction, as shown in Fig. 4, $\dot{\alpha}_y$ = derivative pitch pointing error.

4.1.3. Wheel unloading law

A magnetic torque to off-load the pitch angular momentum during the sun acquisition phase (in Sun submode) is added to ROCSAT-3 design in order to improve SafeHold mode robustness to disturbing torques. During eclipse (in Dark submode), the constant angular momentum h_B is commanded to the wheel on pitch axis so that

$$h_y = -h_B. \tag{8}$$

During this phase, the spacecraft rotates at $2\omega_0$ around the pitch axis.

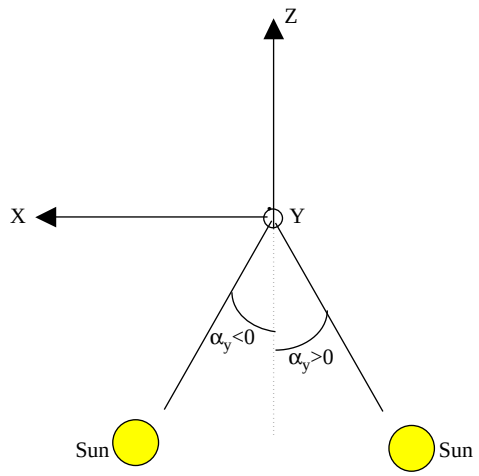

Fig. 4. Sun sensor measurement conventions.

Out of eclipse (in Sun submode), the wheel is used to control spacecraft pitch depointing with respect to the sun so that

$$h_y = -h_B + \Delta h_{acq} + \Delta h_{dist} \tag{9}$$

with $\Delta h_{acq} = -2I_y\omega_0$ = pitch angular momentum variation due to spacecraft stop once sun is acquired.

Δh_{dist} = pitch angular momentum drift due to disturbing torques during sun pointing phase.

Without any particular action, in case of high disturbing torques, the pitch angular momentum drift during sun acquisition may be important. Once in eclipse, the spacecraft rotation (at $2\omega_0$) is longer to establish and requires magnetic torques effect. The solution is to apply a magnetic torque around Y-axis to off-load the wheel. MTQ X and Z, inhibited in Sun submode for attitude control, are commanded for wheel off-loading. MTQ Y still controls X and Z-axes.

The wheel unloading law is

$$\vec{M}_{\text{offload}} = K_{\text{offload}} \cdot \frac{\Delta\vec{h} \times \vec{B}}{\|\vec{B}\|} \tag{10}$$

with

$K_{offload}$ = off-loading control gain,

h_{res} = pitch angular momentum for rescuing the spacecraft rotation at $2\omega_0$ around pitch axis,

$\vec{B}$ = Earth magnetic field measured in the body frame,
$\Delta\vec{h} = \vec{h} - \overrightarrow{h_c}$,
$\overrightarrow{h_c} = (h_B + h_{res})\vec{u}$,
$\vec{u}$ = reference angular momentum direction $[0\ -1\ 0]^T$,
$\vec{h}$ = total angular momentum in spacecraft.

At the end of the sun acquisition phase, when entering eclipse, the angular momentum is commanded to h_B, so that the spacecraft spins instantaneously to $2\omega_0$ thanks to angular momentum control.

4.2. Normal operation mode

The ROCSAT-3 control system provides pitch control by torquing the pitch wheel based on horizon sensor pitch angle data. The pitch wheel torque command is computed from the pitch angle and rate as

$$h_y(t) = K_P\theta + K_{\dot{P}}\dot{\theta}. \tag{11}$$

Roll and yaw control are achieved by commanding the y-axis torque rod based on magnetometer and horizon sensor roll angle data. The electromagnet strength of the torque rod is commanded according to the control law [3]

$$M_y = k_n\dot{B}_y + k_pB_x\phi, \tag{12}$$

where $\dot{B}_y$ is the derivation of the measured magnetic field in the pitch axis, B_x is the measured magnetic field in the roll axis and k_p and k_n are the precession and nutation gain, respectively.

4.3. Orbit control mode

The attitude angles remain small during the burns if the system remains stable, so the equations of motion are derived using small-angle approximations. The burns are short (50–500 s) compared to the orbit period (6000 s), so the orbit angular rate term is neglected. Therefore, from Eq. (4) the satellite equations of motion are

$$I_x\ddot{\phi} - h_B\dot{\psi} = M_x,$$

$$I_y\ddot{\theta} = M_y,$$

$$I_z\ddot{\psi} + h_B\dot{\phi} = M_z. \tag{13}$$

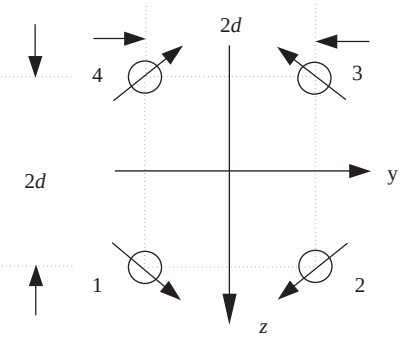

Fig. 5. Thruster mounting geometry.

The four thrusters are mounted in the anti-flight direction of the satellite in each corner of a square with a side length of $2d$, as shown in Fig. 5. The thrusters point primarily along the $+x$-body axis (into the page), but are canted 5° from the x-axis to produce moments about the x-axis. Diagonal pairs are canted in opposite directions. The arrows in Fig. 5 indicate the direction of force generated by each thruster in the body y–z plane. A combination of thrusters 1 and 3 produce a $-x$ torque, while 2 and 4 produce a $+x$ torque. Other thruster combinations produce torques about the y and z-axes (e.g., thrusters 1 and 4 produce a positive torque about the z-axis).

The thrusters are mounted a distance l along the $-x$ axis from the satellite center of mass (and coordinate system origin). The thrusters are canted such that the force vectors are at 45° to the principle axes in the y–z plane. The matrices of thruster force directions and moment arms in the body frame are

$$\vec{F} = \begin{array}{c} \begin{matrix} 1 & 2 & 3 & 4 \end{matrix} \\ \begin{bmatrix} -1 & -1 & -1 & -1 \\ \alpha & -\alpha & -\alpha & \alpha \\ \alpha & \alpha & -\alpha & -\alpha \end{bmatrix} \end{array} \begin{matrix} x \\ y \\ z \end{matrix}$$

$$\vec{r} = \begin{array}{c} \begin{matrix} 1 & 2 & 3 & 4 \end{matrix} \\ \begin{bmatrix} -l & -l & -l & -l \\ -d & d & d & -d \\ d & d & -d & -d \end{bmatrix} \end{array} \begin{matrix} x \\ y \\ z \end{matrix}$$

where $\alpha = 0.707 \times (5°) \times (\pi/180)$.

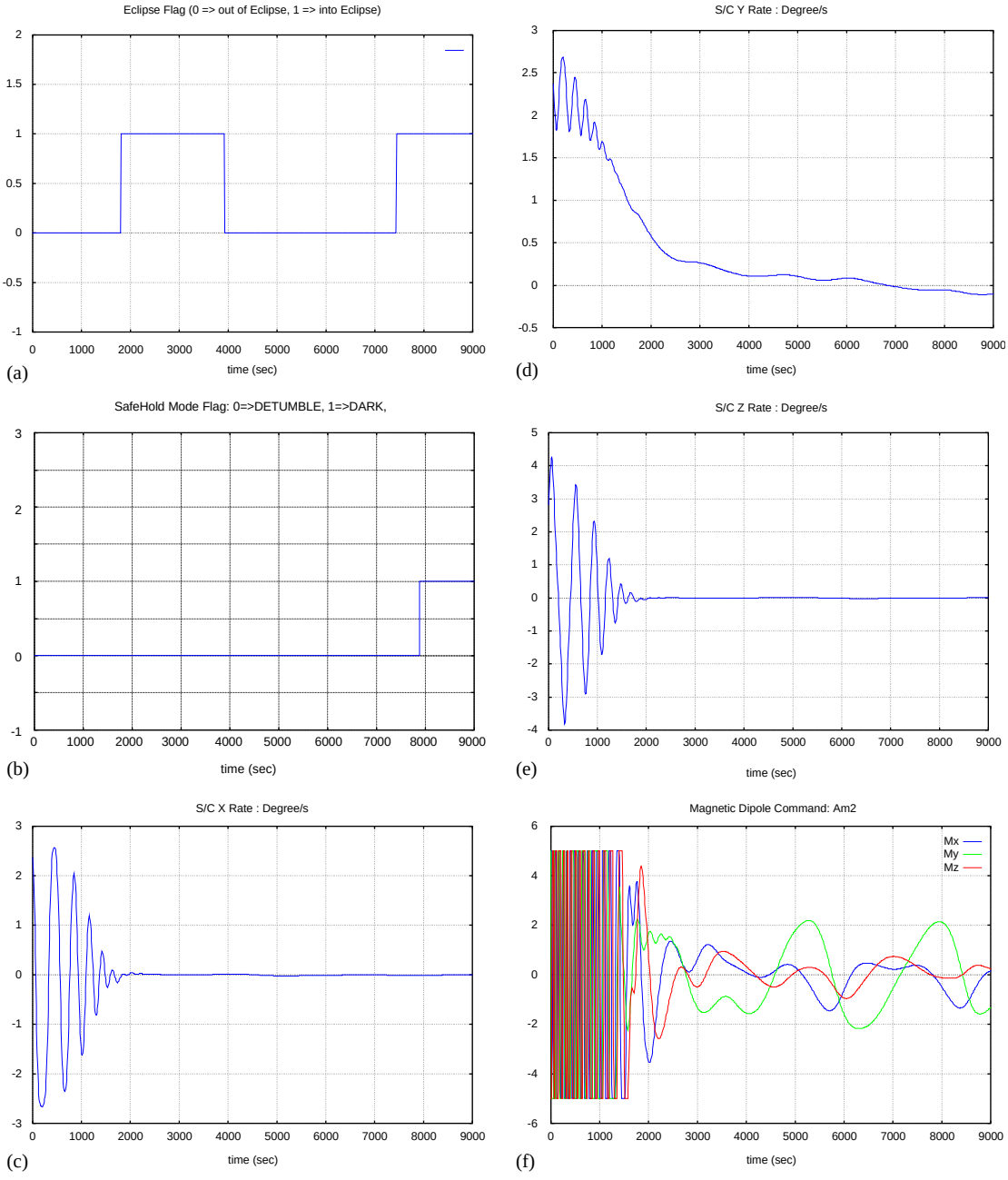

Fig. 6. Performance of Detumble submode.

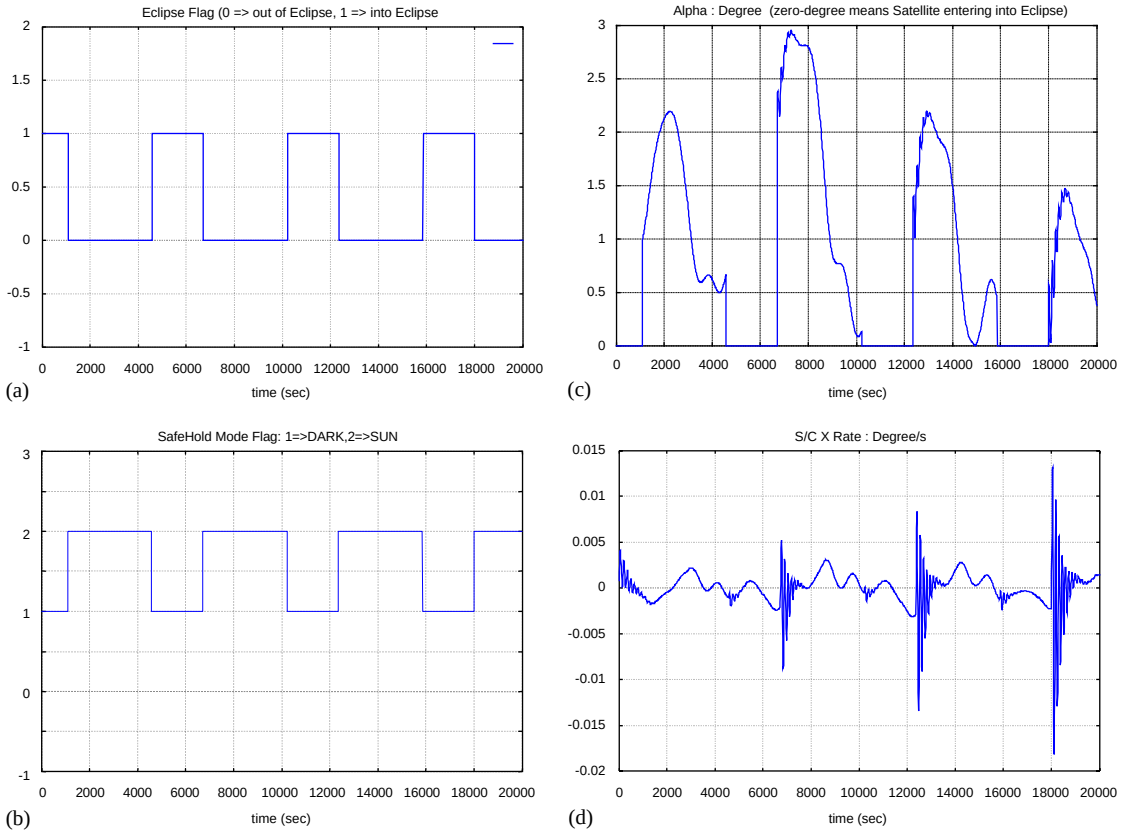

Fig. 7. Performance of Dark and Sun submodes.

The continuous state-space equations of motion are then given by:

$$\begin{bmatrix} \ddot{\phi} \\ \ddot{\theta} \\ \ddot{\psi} \\ \dot{\phi} \\ \dot{\theta} \\ \dot{\psi} \\ \phi \\ \theta \\ \psi \end{bmatrix} = \begin{bmatrix} 0 & 0 & h/I_x & 0 & 0 & 0 & 0 & 0 & 0 \\ 0 & 0 & 0 & 0 & 0 & 0 & 0 & 0 & 0 \\ -h/I_z & 0 & 0 & 0 & 0 & 0 & 0 & 0 & 0 \\ 1 & 0 & 0 & 0 & 0 & 0 & 0 & 0 & 0 \\ 0 & 1 & 0 & 0 & 0 & 0 & 0 & 0 & 0 \\ 0 & 0 & 1 & 0 & 0 & 0 & 0 & 0 & 0 \\ 0 & 0 & 0 & 1 & 0 & 0 & 0 & 0 & 0 \\ 0 & 0 & 0 & 0 & 1 & 0 & 0 & 0 & 0 \\ 0 & 0 & 0 & 0 & 0 & 1 & 0 & 0 & 0 \end{bmatrix} \times \begin{bmatrix} \dot{\phi} \\ \theta \\ \dot{\psi} \\ \phi \\ \theta \\ \psi \\ \int \phi \\ \int \theta \\ \int \psi \end{bmatrix} + \begin{bmatrix} 1/I_x & 0 & 0 \\ 0 & 1/I_y & 0 \\ 0 & 0 & 1/I_z \\ 0 & 0 & 0 \\ 0 & 0 & 0 \\ 0 & 0 & 0 \\ 0 & 0 & 0 \\ 0 & 0 & 0 \\ 0 & 0 & 0 \end{bmatrix}$$

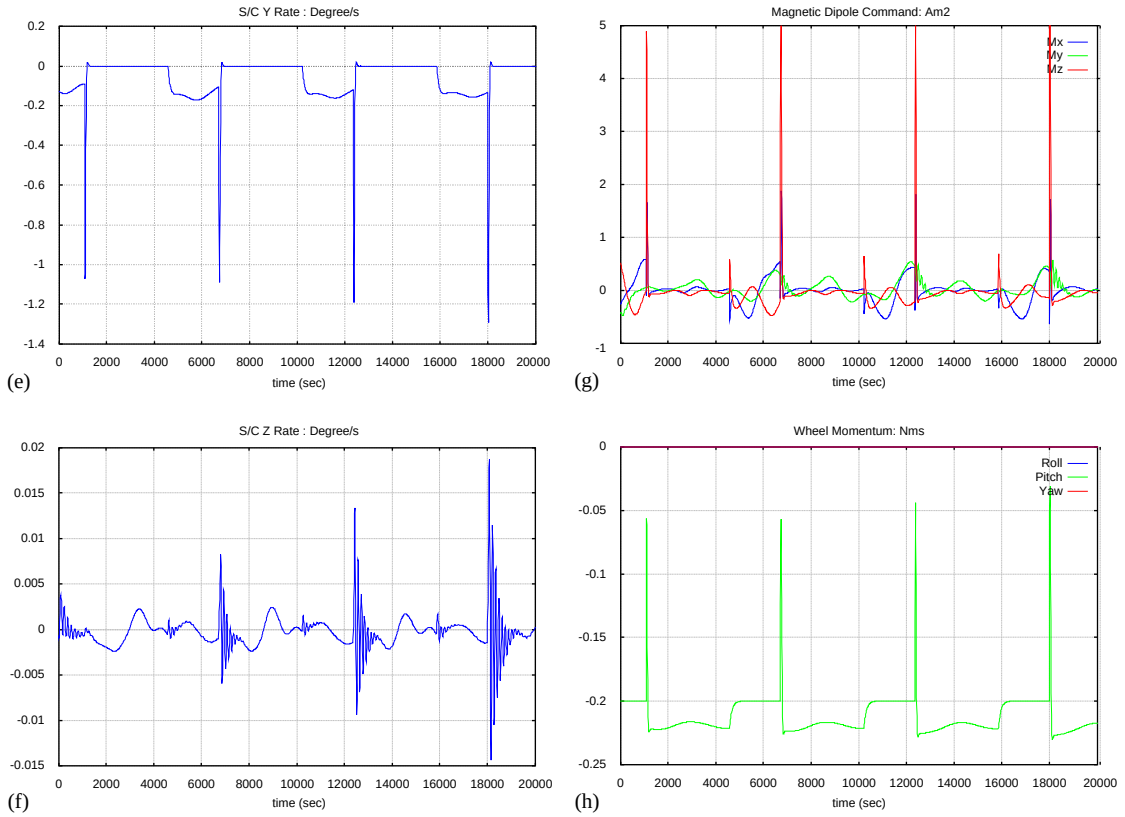

Fig. 7. (*continued*).

$$\times \begin{bmatrix} \vec{r}_1 \times \vec{F}_1 \\ \vec{r}_2 \times \vec{F}_2 \\ \vec{r}_3 \times \vec{F}_3 \\ \vec{r}_4 \times \vec{F}_4 \end{bmatrix}^{\mathrm{T}} \begin{bmatrix} T_1 \\ T_2 \\ T_3 \\ T_4 \end{bmatrix} \tag{14}$$

or

$$\dot{\vec{x}} = A\vec{x} + Bu \tag{15}$$

and T_1–T_4 are the individual thrust levels (a continuum of positive and negative values are required at this point).

The LQR control system uses full-state feedback, where the controller is of the form

$$u(n) = -kx(n), \tag{16}$$

where k is chosen to minimize the cost function

$$J = \tfrac{1}{2} \sum [x^{\mathrm{T}} Q x + u^{\mathrm{T}} R u]. \tag{17}$$

5. Simulation results

5.1. SafeHold mode

The central body inertia are: $Ix = 5.3$ kg m^2, $Iy = 8.5$ kg m^2, $Iz = 4.4$ kg m^2.

5.1.1. Performance of Detumble submode

The simulation presented in this section aims at validating the SafeHold mode Bdot control law convergence with worst case initial conditions (2.5 deg/s per axis).

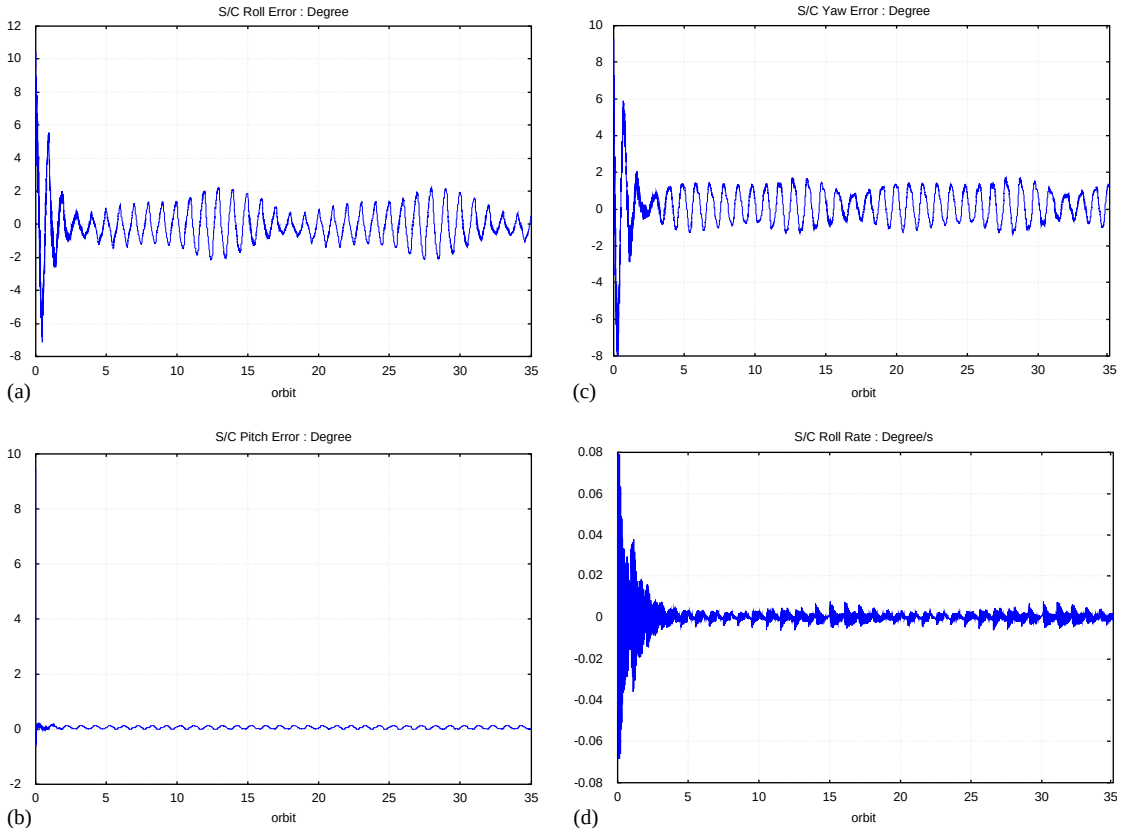

Fig. 8. Performance of normal mode.

Description:

Orbit: parking ($\omega_0 = 1.1 \times 10^{-3}$ rad/s), initial position: 11:50 am LST,

initial attitude: $(\phi\ \theta\ \psi) = (0, 0, 0)$ deg,

initial rates: $(\omega_x\ \omega_y\ \omega_z) = (2.5, 2.5, 2.5)$ deg/s,

wheel momentum bias: -0.2 N m s,

Bdot control gain: $[Kx, Ky, Kz] = [500, 1000, 500]$,

duration: 9000 s.

Results:

- Detumble submode from $t = 0$ to 7880 s: the rates reduction is performed in around 2 orbits (see Figs. 6c–e). The transition from Detumble to Dark is performed when the stabilization counter reaches 1000 s during which convergence criteria $\frac{\vec{B}}{\|\vec{B}\|} < 10^{-3}$ rad/s is fulfilled.
- Dark submode from $t = 7880$ to 9000 s: the spacecraft angular rate around pitch axis (normal to the orbit) is -0.128 deg/s (close to $-2\omega_0$). Dark submode is entered as no sun presence is seen in the sun sensor field of view.

5.1.2. *Performance of Dark and Sun submodes*

The simulation presented in this section aims at validating the sequencing of Sun and Dark submodes and the sun acquisition control law.

Description:

Orbit: operational ($\omega_0 = 1.1 \times 10^{-3}$ rad/s), initial position: 00:00 am LST,

initial attitude: $(\phi\ \theta\ \psi) = (0, 0, 0)$ deg,

initial rates: $(\omega_x\ \omega_y\ \omega_z) = (0, -2\omega_0, 0)$ deg/s.

The initial pitch rate is set close to its converged value in Dark submode (i.e. $-2\omega_0$).

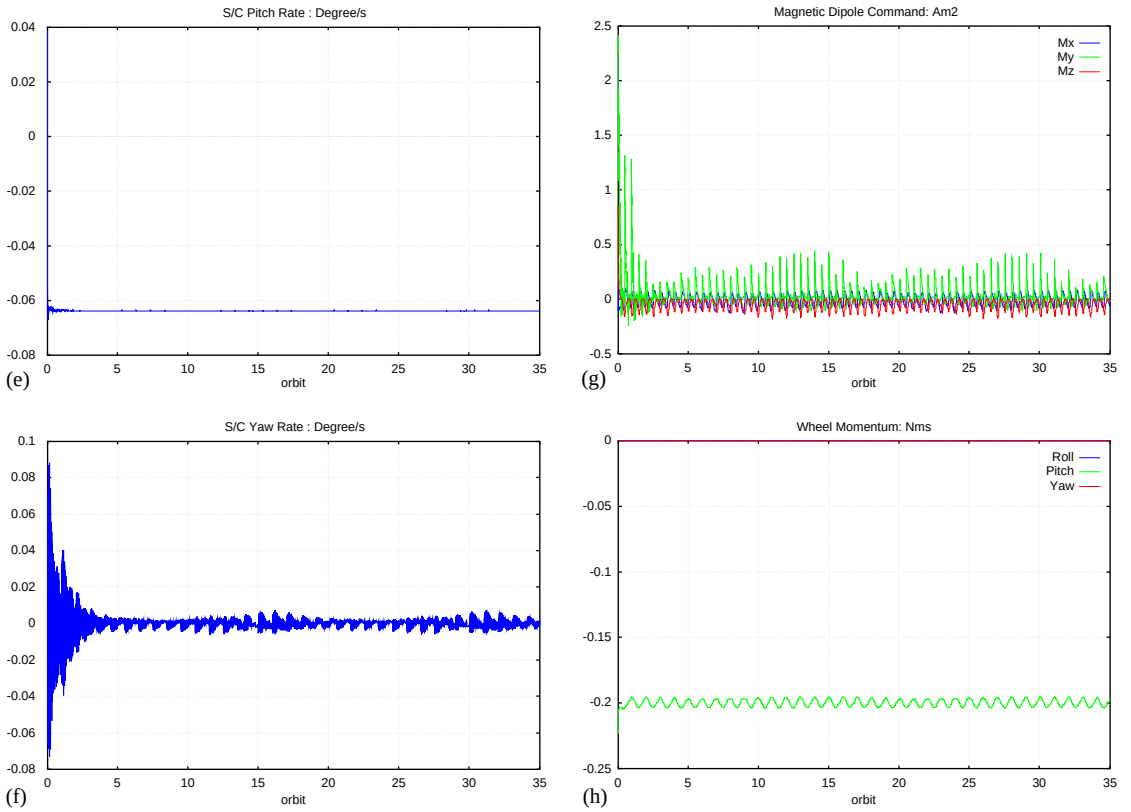

Fig. 8. (*continued*).

Wheel momentum bias: -0.2 N m s,
sun acquisition control gains: $[Ke, Kv]=[0.021, 0.68]$,
wheel unloading gains: $K_{\text{offload}} = 0.001$,
duration : 20,000 s.

Results (Figs. 7a–h):

- Dark submode from $t = 0$ to 1070 s: Dark submode is entered as no sun presence is seen in the sun sensor field of view. Pitch rate is close to $-2\omega_0$ (0.128 deg/s). The sun searching is activated and increases as soon as the Dark submode is entered.
- Sun submode from $t=1070$ to 4580 s: Sun submode is entered as soon as the sun presence is true: the sun presence is true when the sun sensor signal comes in (alpha angle is less than or equal to 90°) then a counter is set to represent the presence of sun. If the counter is set more than 250 s, satellite enters into Sun submode.
- Dark submode from $t = 4580$ to 6710 s: it corresponds to eclipse phase.
- After then, the Sun submode and Dark submode will routinely sequence according to the eclipse and sun light phases.

5.2. Performance of normal mode

The simulation presented in this section is validating the feasibility of utilizing a pitch wheel and a pitch torque rod to control the attitude of the satellite following in nadir-pointing.

Description:
Initial attitude: $(\phi, \theta, \psi) = (10, 10, 10)$ deg,
initial rates: $(\omega_x, \omega_y, \omega_z)=(0.05, -2\omega_0, 0.05)$ deg/s,
wheel momentum bias: -0.2 N m s,
wheel unloading gains: $K_{\text{offload}} = 0.001$,
pitch wheel control gains: $[K_p, K_{\dot{p}}]=[0.037, 0.254]$,
precession and nutation gains: $\lfloor k_p, k_n \rfloor=[5e5, -5e7]$,
duration: 35 orbits (200,000 s).

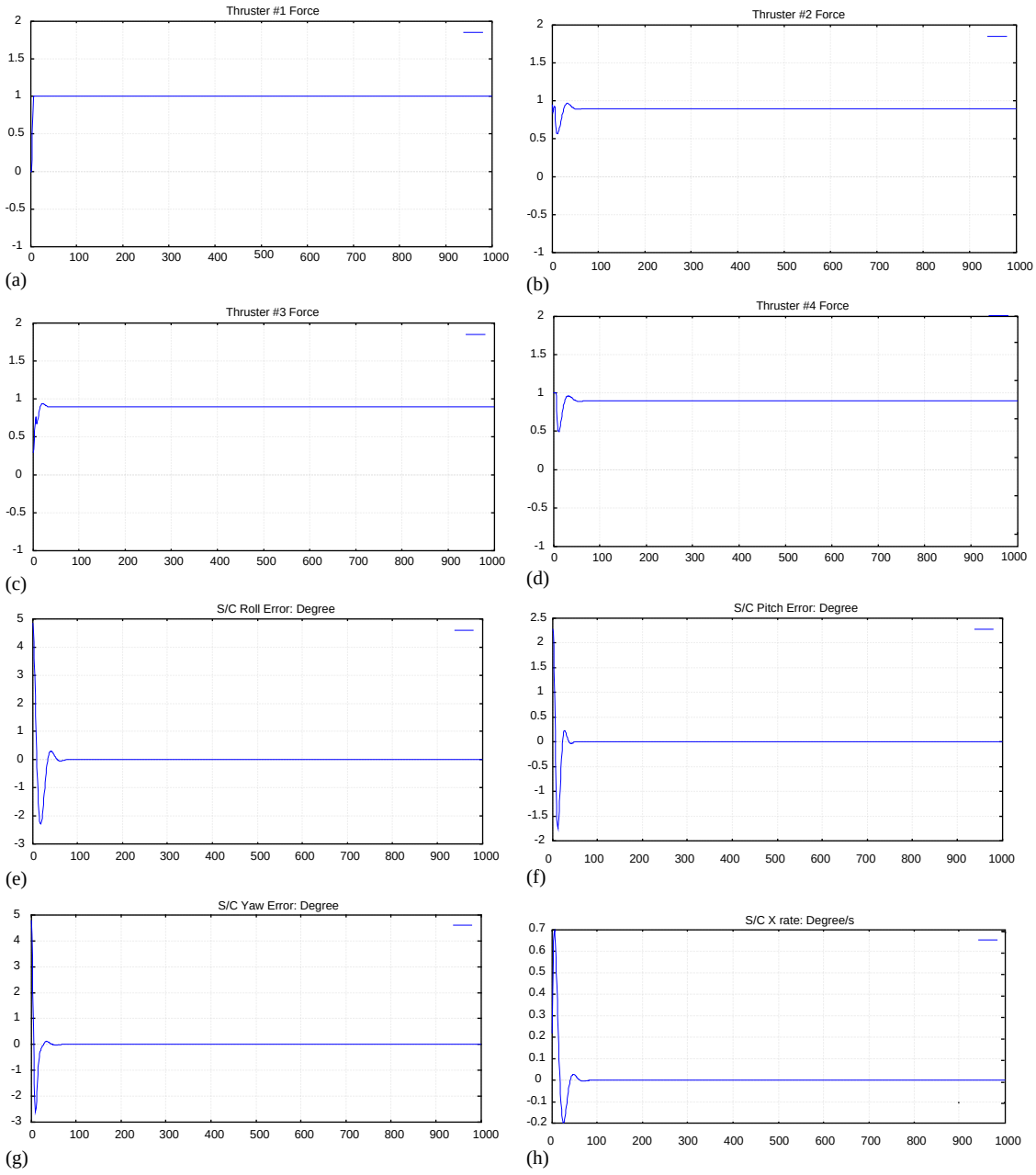

Fig. 9. Performance of orbital control mode.

Results: Fig. 8a–h simulate the normal mode control with an initial spacecraft rate $2\omega_0$ at pitch axis and initial spacecraft attitude errors 10° at each axis. The initial conditions are set to simulate the most likely situation when the control mode is switched from initial and SafeHold mode to normal mode. As we can see from the rate plots, the roll and yaw rates are rapidly reduced to near zero rates and orbit rate at pitch axis.

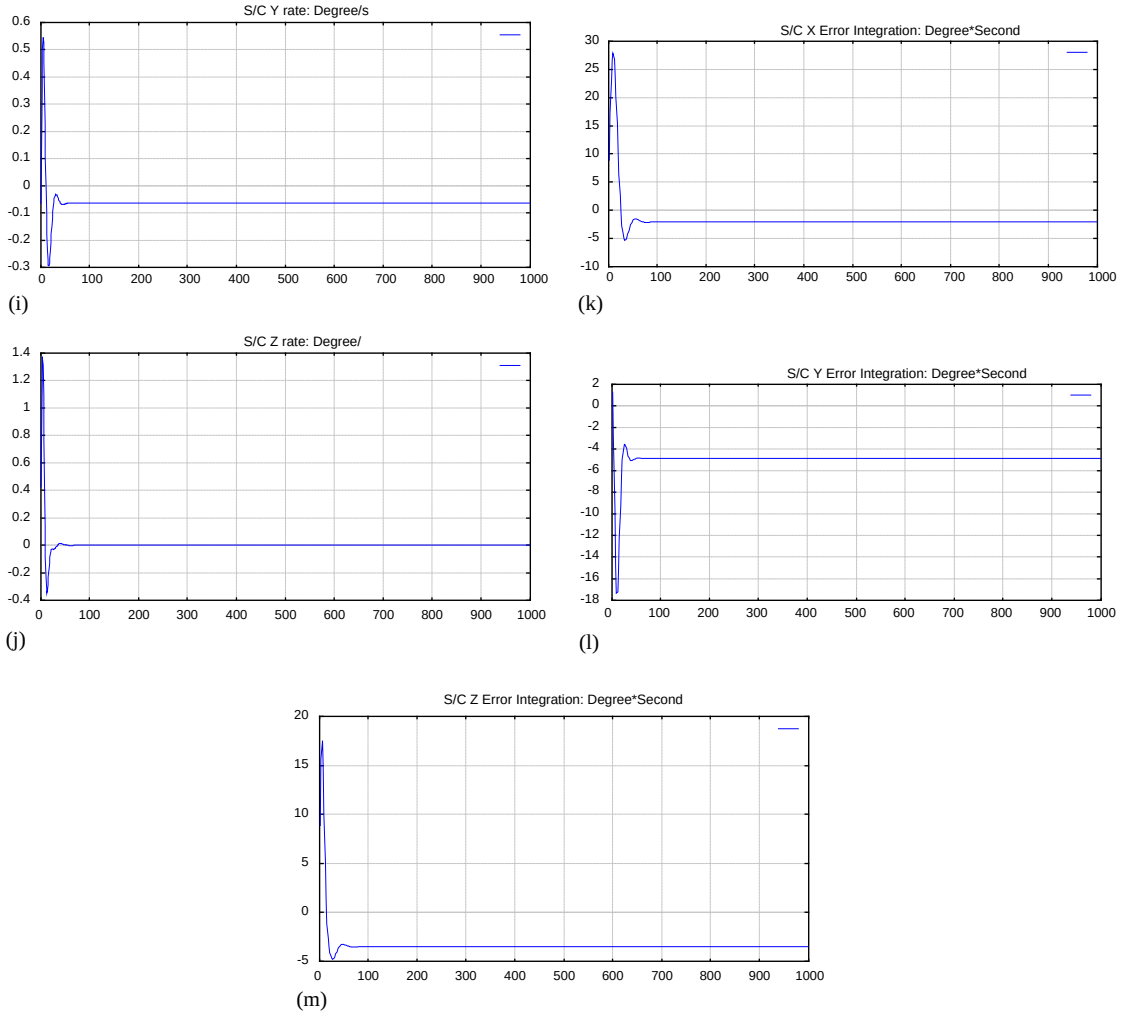

Fig. 9. (*continued*).

The position errors for all three axes meet the 2° pointing at pitch axis and 5° pointing at roll and yaw axes.

5.3. Performance of orbit control mode

The simulation presented in this section is to demonstrate the robustness of the orbit raising control system while the thrust levels are deliberately set as 0.9, 1.0, 1.0 and 1.0 N, respectively.

Description:

Initial attitude: $(\phi, \theta, \psi) = (5, 2, 5)$ deg,

initial rates: $(\omega_x, \omega_y, \omega_z) = (0, 0.2, 0)$ deg/s,

initial wheel momentum: -0.2 N m s.

Matlab® Control System Toolbox, **LQR**, was used to obtain the control gains of Eq. (16) by using Eqs. (15) and (17). The numerical values of satellite parameters and weighting matrix values are:

$d = 0.1$ m	$Q_{11} = Q_{22}$
	$= Q_{33} = 1$—rate weighting
$l = 0.5$ m	$Q_{44} = Q_{55} = Q_{66}$
	$= 1$—angle weighting
$I_{xx} = 5.3$ kg m^2	$Q_{77} = Q_{88} = Q_{99}$
	$= 1$—integral weighting
$I_{yy} = 8.5$ kg m^2	$R_{11} = R_{22} = R_{33} = R_{44}$
	$= 1$—thruster weighting

$I_{zz} = 4.4$ kg m^2
$h = -0.2$ N m s All other Q and R values are zero.

The state weightings (Q's) were chosen by trial and error such that the system was robust to variations in system uncertainties such as thrust level variation, center of gravity (CG) offset and misalignment of thruster. The full-state feedback gain is

$$K = \begin{bmatrix} -32.0243 & -15.6642 & -6.4861 & -4.7606 & -3.9893 & -3.6535 & -0.3581 & -0.5 & -0.6097 \\ 32.0243 & -15.6642 & 6.4861 & 4.7606 & -3.9893 & 3.6535 & 0.3581 & -0.5 & 0.6097 \\ -38.5721 & 15.6642 & 7.0003 & -6.9283 & 3.9893 & 1.4540 & -0.6097 & 0.5 & 0.3581 \\ 38.5721 & 15.6642 & -7.0003 & 6.9283 & 3.9893 & -1.4540 & 0.6097 & 0.5 & -0.3581 \end{bmatrix}.$$

The corresponding closed-loop roots in the s-plane are:

$$S = -0.2043 \pm j0.3380, -0.0849 \pm j0.1432, -0.1295 \pm j0.2193, -0.3790, -0.1675, -0.2509.$$

Thrust level: $(F1, F2, F3, F4) = (0.9, 1.0, 1.0, 1.0)$ N, duration: 1000 s.

Results: Figs. 9a–d show the command force time history for the situation of deficient thrust level. Thruster 1 fired during the entire burn while the other three thrusters reached a steady-state of 0.9 of normal value. This is to reflect the fact that the thruster 1 was set to produce 10% less thrust than the others and the normal thrusters must fire with smaller thrust to produce the same torques as the deficient one. As for Figs. 9e–m show the response of the nine state variables.

6. Conclusion

The ROCSAT-3 attitude control subsystem has been conceptually designed to meet the weight and power constraints of a microsatellite with complicate mission demands. The proposed control schemes for the three control modes and the spacecraft attitude dynamics were analyzed to demonstrate the satisfaction of the required performances. The attitude control subsystem is used during the orbit transfer phase and for nominal science operations in the final orbit. Sensors and actuators have been selected to accommodate both mission phases. As a result, the ROCSAT-3 attitude control subsystem design is versatile, robust and affordable.

References

[1] R. Ware, GPS sounding of the atmosphere from low earth orbit: preliminary results, Bulletin of the American Meteorological Society 77 (1) (1996) 19–40.
[2] J.R. Wertz, Spacecraft Attitude Determination and Control, Kluwer Academic Publishers, Boston, 1990.
[3] C. Stickler, K.T. Alfriend, Elementary magnetic attitude control system, Journal of Spacecraft and Rockets 13 (5) (1976) 282–287.